

Numerical simulation of the coupled flutter instability for closed-box bridge decks

Giovanni Cannata, Luca Barsi, and Francesco Gallerano

Abstract—In this work a numerical investigation of aeroelastic phenomena for long-span bridge decks is proposed: a simulation model is presented by which the aerodynamic fields and the motion of the structure are simulated simultaneously and in a coupled manner. The structure is represented as a bidimensional elastically suspended rigid body with two degrees of freedom, and the aerodynamic fields are simulated by numerically integrating the ALE formulated 2D URANS equations with a finite volume scheme on moving grids which adapt to the structural motion. The numerical model is validated by the comparison between numerical and experimental results, and is utilised to study the aeroelastic stability of the Forth Road Bridge deck. A deep insight into the onset and the amplification mechanisms of coupled flutter for long span bridge decks is proposed. The numerical model is also used to test the effectiveness of a small aerodynamic modification on the aeroelastic stability of the deck.

Keywords—Bridge aeroelasticity, finite volume, moving grids, turbulence modelling.

I. INTRODUCTION

FLUTTER is an oscillatory aero-elastic phenomenon to which long-span bridge decks are prone. Once the instability is triggered, the amplitudes of oscillation increase fast and the bridge deck is rapidly driven to collapse [1]. Torsional flutter can affect bridge decks with bluff cross-section, as it has been seen in the case of the Tacoma Narrows Bridge deck, and its physical mechanism has been widely investigated by many research groups. It has been recognized that the key to the torsion instability mechanism is the formation and drift of large-scale vortices on the cross-section of the deck [2, 3]. Coupled (torsional-flexural) flutter can involve bridge deck with streamlined cross-section. The risk of coupled flutter is significant if the torsional natural frequency is only slightly larger than the vertical natural frequency, which is usually the case of long-span bridge decks [4]. Bridge deck coupled flutter has been experimentally investigated in [5]. The latter authors distinguish a torsional-branch (TB)

coupled flutter and a heaving-branch (HB) coupled flutter. TB coupled flutter looks like a fundamentally torsional motion, with the rotational axis at a certain point apart from mid-chord point. HB coupled flutter looks like a mainly heaving motion with large amplitude, accompanied by a torsional motion with small amplitude.

The identification of the critical flutter wind velocity of bridge decks is usually performed by means of the Scanlan method [6]. In this method, which rests on the assumption of sinusoidal oscillations, the forces produced by the aerodynamic fields on the deck are modelled as linear functions of the structural displacements. This is accomplished by using a set of parameters, named *flutter derivatives*, which can be either estimated numerically and experimentally. As underlined in [7] and [1], the linear relationship between the aerodynamic forces and the structural displacements turns out to be adequate only if the deck oscillations have small amplitudes. The same authors stress that this linear relationship does not permit to consider the effects of the unsteady vortices generated by the wind-structure interaction.

By contrast, many authors [4, 8-10] identify the critical flutter wind velocity by the free motion procedure. In this procedure, the aerodynamic fields and the structural motion are simultaneously and jointly simulated, so that the aeroelastic stability is verified for various wind speeds directly. According to this procedure, the pressure and velocity fluid fields that develop around the structure at every instant are simulated; starting from the aerodynamic pressures, the lift force and the twisting moment acting on the structure at every instant are computed; once the above-mentioned aerodynamic forces are known, the structural displacements are calculated; these displacements, in turn, modify the computational domain and the boundary for numerical integration of the fluid motion equations and, as a consequence, modify the structure of the aerodynamic fields. With respect to the Scanlan method, the free motion procedure provides more useful insights into the physical mechanisms of the aeroelastic instability.

Finite volume techniques are used by many authors in order to simulate the aerodynamic fields on unstructured grids [11-13] or on structured grids [14-18]. Many authors [19-21] underline that, when the aerodynamic fields are simulated around moving objects, the Arbitrary Lagrangian Eulerian (ALE) formulation has to be applied to the fluid motion equations.

The instabilities of the decks are related to the unsteady

G. Cannata is with the Department of Civil, Constructional and Environmental Engineering, "Sapienza" University of Rome, Via Eudossiana, 18, 00184 Rome, (corresponding author to provide phone: +39 0644585062; e-mail: giovanni.cannata@uniroma1.it).

L. Barsi is with the Department of Civil, Constructional and Environmental Engineering, "Sapienza" University of Rome, Via Eudossiana, 18, 00184 Rome, (e-mail: luca.barsi@uniroma1.it).

F. Gallerano is with the Department of Civil, Constructional and Environmental Engineering, "Sapienza" University of Rome, Via Eudossiana, 18, 00184 Rome, (e-mail: francesco.gallerano@uniroma1.it).

phenomena of the aerodynamic fields [2, 22, 23], and in particular to the formation of unsteady vortex structures. The URANS approach makes it possible to simulate the quasi-periodic unsteady vortex structures of the aerodynamic field [24] and (with reference to aeroelastic instability phenomena such as vortex induced vibrations and flutter) to well identify the onset velocities and the amplitudes of the induced structural oscillations [25].

In this work the aeroelastic stability of long-span bridge decks is numerically investigated. A simulation model is presented by which the aerodynamic fields and the structural motion are simultaneously and jointly simulated. The bridge deck is schematised as a bidimensional rigid body subject to elastic restraints corresponding to the torsional and the vertical degree of freedom, and the ALE formulated 2D URANS equations are numerically integrated by a finite volume technique on meshes which deform according to the motion of the structure. The finite volume technique is based on high order weighted essentially non-oscillatory (WENO) reconstructions, and the advancing in time of the solution is carried out through a five stage fourth order accurate strong stability preserving Runge-Kutta (SSPRK) method. By the proposed numerical method it is possible to ensure high accuracy both in space and time. The URANS equations are completed by the turbulent closure relations which are expressed as a function of the turbulent kinetic energy, the turbulence frequency and the strain tensor according to the $k-\omega$ SST approach. The proposed model is applied to the case study of the Forth Road Bridge deck in its current configuration, and is validated by comparing the obtained numerical results with those of an experimental campaign [15]: in order to perform the above validation, the critical flutter wind velocity and the root mean square of rotational displacements are taken as benchmark parameters. A profound insight into the onset and the amplification mechanisms of coupled flutter for long-span bridge decks is proposed. Such profound insight makes it possible to deduce that the reason for the coupled flutter onset lies in the fact that, within each of the first oscillation cycles, there is a portion of the cycle in which the energy supplied by the aerodynamic field to the deck motion is more than the energy extracted in the rest of the cycle. Moreover, it is deduced that the reason for the amplification of the aeroelastic instability is ascribable to the formation and drift of large vortical formations along the surface of the deck. The proposed model is also used in order to test the effectiveness, on the aeroelastic stability of the deck, of the introduction of a couple of sloping barriers at the windward and leeward bridge deck edges. The differences in the static behaviour exhibited by the deck in the current and the modified configuration are highlighted by comparing the time-averaged static coefficients (drag, lift and moment coefficient) and the Strouhal number related to both cases. The detailed analysis of the aerodynamic fields and the structural motion makes it possible to highlight the differences produced by the introduction of the sloping barriers in the evolutionary

dynamics of the vortices generated in the fluid-structure interaction. It is demonstrated that this small aerodynamic modification is effective in increasing the critical flutter wind velocity and mitigating the vibration amplitudes which develop during the flutter instability.

II. THE PROPOSED MODEL

A. The Fluid Motion Equations

The simulation of the aerodynamic field is performed by numerically integrating the ensemble averaged continuity and momentum equations. In integral form, the ALE (Arbitrary Lagrangian-Eulerian) formulated 2D URANS (Unsteady Reynolds-Averaged Navier-Stokes) equations are expressed as follows [26]:

$$\frac{d}{dt} \int_{\Delta A} dA + \int_L [\langle u_i \rangle - u_{g,i}] n_i dL = 0, \quad (1)$$

$$\begin{aligned} \frac{d}{dt} \int_{\Delta A} \langle u_i \rangle dA = & - \int_L \langle u_i \rangle [\langle u_j \rangle - u_{g,j}] n_j dL \\ & + \int_{\Delta A} \frac{\partial}{\partial x_j} [2\nu \langle S_{ij} \rangle - \langle u_i' u_j' \rangle] dA + \int_{\Delta A} f_i dA - \int_{\Delta A} \frac{\partial \langle P \rangle}{\partial x_i} dA. \end{aligned} \quad (2)$$

being $\langle u_i \rangle$ and $\langle P \rangle$ respectively the ensemble-averaged i -th fluid velocity component and the ensemble-averaged fluid pressure, $u_{g,i}$ the i -th grid velocity component, ν the kinematic fluid viscosity, f_i the i -th component of the mass force vector, dA the surface area of an element delimited by the contour line L , and n_j the normal pointing outward. The additional unknown $\langle u_i' u_j' \rangle$, which can be defined as the Reynolds tensor, is modelled based on the Boussinesq assumption:

$$\langle u_i' u_j' \rangle = -2\nu_t \langle S_{ij} \rangle + \frac{2}{3} \langle k \rangle \delta_{ij}, \quad (3)$$

being $\langle S_{ij} \rangle$ the ensemble averaged strain rate tensor, $\langle k \rangle$ the ensemble averaged turbulent kinetic energy per unit mass, ν_t the kinematic eddy viscosity, δ_{ij} the Kronecker symbol. The turbulent closure relations adopted in this work, together with the calibration parameters herein included, are taken from [27].

B. The Structural Motion Equations

By neglecting the displacements in the horizontal direction x , the 2D motion of the body can be described in terms of two displacement components, η , θ , where η is the translational displacement of the gravity centre in the vertical direction y , and θ is the torsional displacement of the body (rotation). The governing equations for the body motion are expressed as follows:

$$m\ddot{\eta} + S\ddot{\theta} + c_y\dot{\eta} + k_y\eta = f_y(\eta, \dot{\eta}, \ddot{\eta}, \theta, \dot{\theta}, \ddot{\theta}), \quad (4)$$

$$I\ddot{\theta} + S\dot{\eta} + c_\theta\dot{\theta} + k_\theta\theta = m_\theta(\eta, \dot{\eta}, \ddot{\eta}, \theta, \dot{\theta}, \ddot{\theta}), \quad (5)$$

being f_y and m_θ the vertical component of the aerodynamic force and the twisting moment generated by the same force, m and I the structural mass and the structural moment of inertia per unit length, S the static imbalance (which is equal to m times the distance a between the shear centre and the centre of mass), c_y and c_θ the structural damping constants in the vertical and torsional degree of freedom, and k_y and k_θ the stiffness constants of the vertical and the torsional elastic spring. The integration of the pressures, the viscous stresses and the turbulent stresses over the surface of the structure allows the calculation of the force component f_y and the twisting moment m_θ . The stiffness constants are ascribed to give the correct natural frequencies in the fundamental flexural and torsional modes of vibration of the structure. The damping coefficients are derived from the known damping ratios by means of the classical viscous damping assumption. The structural motion equations are solved by a second-order accurate scheme, and the coupling between the fluid solver and the structure solver follows a partitioned loose-coupling approach [28].

C. The Numerical Scheme

In this section we present the finite volume method used for the numerical integration of the fluid motion equations.

Let us define $\langle \bar{u}_i \rangle$ and $\langle \bar{P} \rangle$ as the cell averaged values of the velocity vector and the pressure:

$$\langle \bar{u}_i \rangle = \frac{1}{\Delta A} \int_{\Delta A} \langle u_i \rangle dA, \quad \langle \bar{P} \rangle = \frac{1}{\Delta A} \int_{\Delta A} \langle P \rangle dA. \quad (6)$$

The state of the system is known at the centre of the calculation cell and it is defined by the cell-averaged values $\langle \bar{u}_i \rangle$ and $\langle \bar{P} \rangle$. The time level at which the variables are known is n , while the time level at which the variables are unknown is $n+1$. From the values of the fluid dynamic quantities at the time $t^{(n)}$, by solving the structural motion equations, the structural displacements are calculated and, from the latter, the coordinates of the control volume vertices are updated and the grid velocity $u_{g,i}^{(n)}$ is calculated. Given the values of $\langle \bar{u}_i \rangle^{(n)}$, $\langle \bar{P} \rangle^{(n)}$, $\langle \bar{\kappa} \rangle^{(n)}$, $\langle \bar{\omega} \rangle^{(n)}$ at the centre of the calculation cells at the time $t^{(n)}$, the calculation of the values of $\langle \bar{u}_i \rangle^{(n+1)}$, $\langle \bar{P} \rangle^{(n+1)}$, $\langle \bar{\kappa} \rangle^{(n+1)}$, $\langle \bar{\omega} \rangle^{(n+1)}$ at the time $t^{(n+1)}$ is performed by integrating the fluid motion equations (supplied with the turbulence closure relations for the Reynolds stress tensor).

In the solution procedure for the fluid motion equations, a five stage fourth order accurate Strong Stability Preserving Runge-Kutta (SSPRK) fractional-step method is used for the momentum equations and a pressure correction formulation is applied to obtain a divergence free velocity field at each time level. Having indicated with $\langle \bar{u}_i \rangle^{(n)}$ the value of the i -th component of the fluid velocity field at the time level n , the following five stage iteration procedure is adopted in order to calculate the fluid velocity field $\langle \bar{u}_i \rangle^{(n+1)}$ at the time level $n+1$.

Let be

$$\langle \bar{u}_i \rangle^{(0)} = \langle \bar{u}_i \rangle^{(n)}. \quad (7)$$

At each stage p (where $p = 1, 2, \dots, 5$), an intermediate velocity field $\langle \bar{u}_i \rangle^{*(p)}$ is obtained explicitly through (2) by using the values of the previous time level

$$\langle \bar{u}_i \rangle^{*(p)} = \sum_{q=0}^{p-1} \left[\Omega_{pq} \langle \bar{u}_i \rangle^{(q)} + \Delta t \varphi_{pq} D \left[\langle u_i \rangle^{(q)}, t^{(n)} + d_q \Delta t \right] \right], \quad (8)$$

being $D(\langle u_i \rangle, t)$ equal to the right-hand side of (2) divided for ΔA , in which the pressure gradient term has been ignored. For the values of the coefficients Ω_{pq} , φ_{pq} and d_q refer to [29]. In general, the requirement to satisfy the continuity equation is not met by the intermediate velocity field of (8). Therefore, the velocity and the pressure field are corrected as follows. By introducing a scalar potential Ψ , the well-known Poisson pressure equation in integral form reads:

$$\int_L \frac{\partial \Psi^{(p)}}{\partial x_i} n_i dL = - \int_L \langle \bar{u}_i \rangle^{*(p)} n_i dL, \quad (9)$$

where L and n_i are respectively the contour of the calculation cell and the i -th component of the unit outward vector normal to the contour. The calculation of the above scalar potential Ψ is performed by solving (9). The corrector velocity field $\langle \bar{u}_i \rangle^c$ is calculated by means of the relation

$$\langle \bar{u}_i \rangle^c = \frac{\partial \Psi^{(p)}}{\partial x_i}. \quad (10)$$

The velocity field $\langle \bar{u}_i \rangle^p$ at the stage p is given by

$$\langle \bar{u}_i \rangle^{(p)} = \langle \bar{u}_i \rangle^{*(p)} + \langle \bar{u}_i \rangle^c. \quad (11)$$

The velocity and pressure fields at the time $t^{(n+1)}$ are respectively given by

$$\langle \bar{u}_i \rangle^{(n+1)} = \langle \bar{u}_i \rangle^{(5)}, \quad \langle \bar{P} \rangle^{(n+1)} = \frac{1}{\Delta t} \Psi^{(5)}. \quad (12)$$

The calculation of the term $D(\langle u_i \rangle, t)$ require the numerical approximations of the integrals on the right-hand side of (2). This calculation is based on the following passages:

1. High order WENO reconstructions, from cell averaged values, of the point values of the unknown variables at the centre of the contour segments which define the calculation cells. At the centre of the contour segment which is common with two adjacent cells, two point values of the unknown variables are reconstructed by means of two WENO reconstructions defined on two adjacent cells.

2. Advancing in time of the point values of the unknown variables at the centre of the contour segments by means of the so-called exact solution of the Riemann problem, with initial data given by the pair of point values computed by two WENO reconstructions defined on the two adjacent cells.

3. Calculation of the spatial integrals which define $D(\langle u_j \rangle, t)$.

Further details regarding the WENO reconstructions, the advancing in time of the unknown variables and the calculation of the spatial integrals which define $D(\langle u_j \rangle, t)$ can be found in [30-32]. The numerical integration of the turbulence closure relations makes it possible to calculate $\overline{\langle k \rangle}^{(n+1)}$, $\overline{\langle \omega \rangle}^{(n+1)}$ and the Reynolds stress tensor at the time $t^{(n+1)}$ through (3). The discretisation of (8) and (9) by means of the numerical method introduced above entails the risk of introducing mass sources or sinks in the flow field, if the grid velocity $u_{g,i}$ and the change of volume over time are not treated consistently. For this reason, the Geometric Conservation Law (GCL)

$$\frac{d}{dt} \int_{\Delta A} dA + \int_{\Delta A} \frac{\partial u_{g,i}}{\partial x_i} dA = 0 \quad (13)$$

has to be satisfied. In order to warrant consistency, (13) is used to determine the grid velocity by the given change of volume of the computational cell [26]. In order to update the coordinates of the control volume vertices at all times, a mesh movement algorithm based on using Inverse Distance Weighting [33] is used in order to interpolate the displacements of the boundary nodes to the whole flow mesh.

III. RESULTS AND DISCUSSION

In this section, the proposed simulation model is utilised to analyse the full fluid-structure interaction of the Forth Road Bridge deck in the current configuration. Table 1 lists the full-scale geometric and structural properties used in the fluid-structure interaction analysis, which are taken from [9]. In Fig. 1 the geometric characteristics of the Forth Road Bridge deck cross-section in the current configuration are shown.

Table1: full-scale properties of the Forth Road Bridge deck

Overall width (B)	31.2 m
Maximum depth (D)	3.2 m
Unit length mass (m)	17.3×10^3 kg/m
Unit length moment of inertia (I)	2.13×10^6 kgm ² /m
Heaving natural frequency (f_v)	0.174 Hz
Torsional natural frequency (f_θ)	0.4 Hz
Heaving damping ratio (c_v)	0.31%
Torsional damping ratio (c_θ)	0.14%

A. Geometry and Numerical Modelling

The results related to the bridge deck in its current configuration are obtained by using a block-structured grid which is made up of 272464 cells. In this grid, a geometric progression of 1.02 for the cell size varying is used in all directions. The dimensions of the computational domain in the

x and y directions are respectively equal to $Dx = 10B$ e $Dy = 5B$ (being B the width of the cross-section of the deck). In each simulation, the adopted Reynolds number correspond to that derived from the full-scale wind velocity U , the air kinematic viscosity ν (which is equal to 1.23×10^{-5} m²/s) and the cross-section width B . The time step is derived by imposing the Courant number to be less than 0.9 in all the simulations: e.g., for the simulation performed at $Re = 1.95 \times 10^8$ ($U = 87.4$ m/s) this prescription produces a minimum time step close to $\Delta t = 1 \times 10^{-5}$ s.

For the fluid pressure, a zero gradient boundary condition is applied at the inflow of the domain, while at the domain outlet a constant pressure boundary condition is applied. For the other quantities (fluid velocity, turbulent kinetic energy and turbulence frequency) a constant value is imposed at the inflow, while a zero gradient boundary condition is applied for the same quantities at the outlet. The near-wall treatment proposed in [34], which permits to switch automatically from a classical low-Re formulation on fine grids to a wall function formulation on coarser meshes, is used at the solid walls.

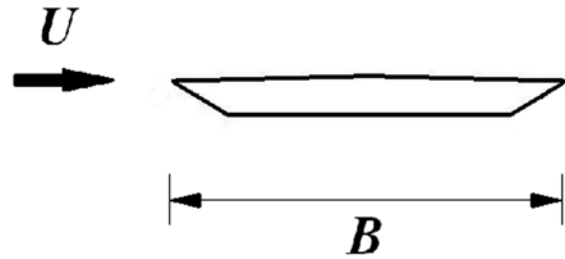


Fig. 1: Geometry of the Forth Road Bridge deck cross-section in the current configuration

B. Model Validation

The model validation is performed by comparing the numerical results with those obtained from the wind tunnel tests described in [9]. Fig. 2 shows the plot of the damping coefficient of the rotations against the reduced velocity U_θ of the wind ($U_\theta = U / (f_\theta B) = 6.34$, being f_θ the natural torsional frequency of the deck). From Fig. 2 it can be observed that the reduced critical velocity obtained by the proposed model is $U_\theta^* = 6.34$ (which corresponds to a full-scale critical wind velocity of 79.1 m/s). This value matches very well the experimental result of $U_\theta^* \approx 6.35$ reported in [9]. Fig. 3 shows the plot of the root mean square of the rotations against the reduced velocity U_θ . In this figure, both the root mean square values obtained numerically in the present work and the experimental ones taken from [9] are shown. By observing Fig. 3 it can be seen that the numerical results are in good agreement with the experimental ones. Lastly, the frequencies of the rotational and the vertical motion of the deck are identified for the considered reduced velocities U_θ . In agreement with that reported in [9], it is found that at the point of flutter instability the frequencies of the translational and rotational motion are identical. In particular, the

synchronization frequency is found to be $f_{\theta}^* = 0.34$ Hz.

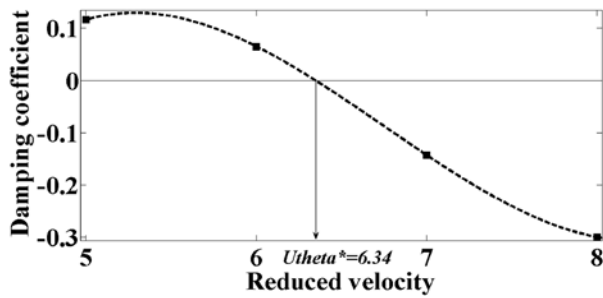


Fig. 2: Damping coefficients of the rotations against the reduced velocity

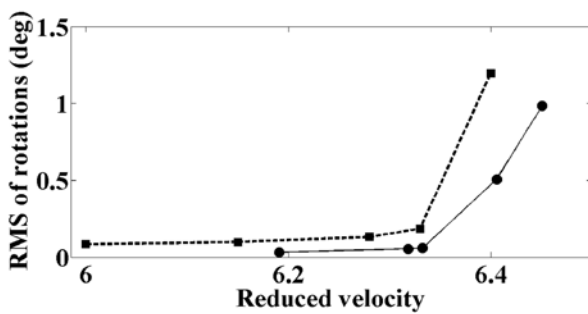


Fig. 3: Root-mean-square of the rotations against the reduced velocity

C. Flutter Type Characterization

According to [5], the type of flutter affecting the Forth Road Bridge is characterised by means of the angle Ψ defined as the phase delay of the deck heaving response (vertical displacements) to the deck torsional response (rotations). These authors underline that the oscillatory motion of the cross-section of a bridge deck can be seen as the overlapping of two fundamental oscillatory motions. The first of these motions is named as *torsional fundamental mode* and mainly consists of a pure rotational motion around a certain point apart from the mid-chord point. In this first mode, the angle Ψ is equal to 0° (Fig. 4) or 180° (Fig. 5) depending on whether the centre of rotation is placed upstream or downstream the mid-chord point of the deck cross-section. The second of the above fundamental motions is named as *heaving fundamental mode* and consists of a prominent heaving motion with the accompany of small torsional oscillations. In this second mode, the angle Ψ is equal to 90° (Fig. 6) or -90° (Fig. 7) depending on whether the sign of the small rotation of the upward moving cross-section is clockwise or anti-clockwise during the passage from the position of static equilibrium to a position of maximum relative height.

Having introduced the flutter fundamental modes, the above authors distinguish a torsional-branch (TB) coupled flutter and a heaving-branch (HB) coupled flutter. In particular, the

coupled flutter is of TB type if the torsional fundamental mode dominates on the heaving fundamental mode. In the case under examination (Forth Road Bridge), the angle Ψ is found to be equal to -16° , so that the relative contribution of the torsional and the heaving fundamental mode can be respectively quantified as $|\cos(-16^\circ)| = 0.96$ and $|\sin(-16^\circ)| = 0.27$. It is thus concluded that the Forth Road Bridge deck is prone to a TB coupled flutter in which the torsional fundamental mode clearly dominates the heaving fundamental mode.

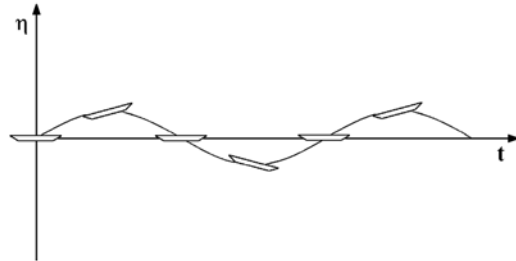


Fig. 4: Torsional fundamental mode, $\Psi = 0^\circ$

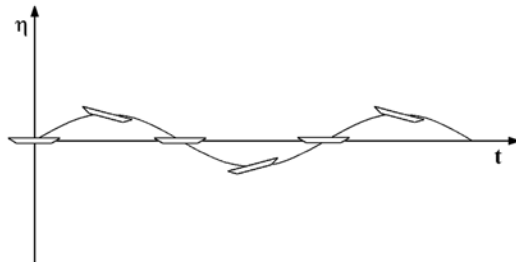


Fig. 5: Torsional fundamental mode, $\Psi = 180^\circ$

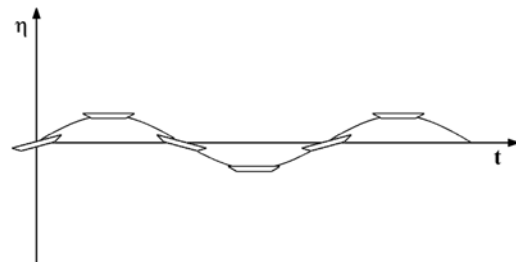


Fig. 6: Heaving fundamental mode, $\Psi = 90^\circ$

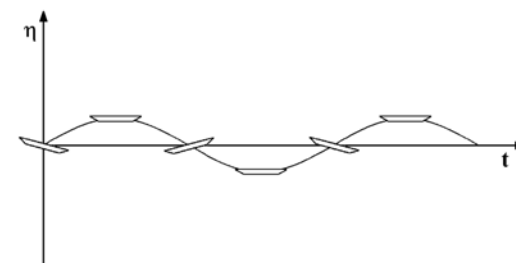


Fig. 7: Heaving fundamental mode, $\Psi = -90^\circ$

D. Coupled Flutter Onset Mechanism

Below the onset mechanism of coupled flutter is shown. For this purpose, the evolution of the aerodynamic forces and the structural displacements produced for a wind speed $U = 87.4$ m/s ($U_\theta = 7.0$) is investigated during a cycle of structural oscillations in which the amplitudes of vibration are still limited. Fig. 8 shows together the time history of the resultant of the unit-area forces exerted by the fluid on the deck surface and the time history of the infinitesimal vertical displacement of the centre of gravity of the deck. Fig. 9 shows together the time history of the twisting moment produced by the above resultant force and the time history of the infinitesimal deck rotation. The structural oscillation cycle shown in Figs. 8, 9 is delimited by two time instants (indicated as A and E) at which a relative minimum value is assumed by the infinitesimal vertical displacement of the downward moving gravity centre of the structure.

- By observing Fig. 8 it is deduced that in the time interval between instants A and B the gravity centre moves downward and passes from the position which corresponds to the static equilibrium to the position of minimum height (within the considered cycle), when the vertical velocity of the gravity centre of the structure vanishes. In this interval the resultant of the aerodynamic forces is directed upward, thus acting in opposition to the downward translational motion of the deck and, consequently, provides a damping effect on the same translational motion.
- In the time interval between instants B and C the gravity centre of the structure inverts the direction of the translational motion and passes from the position of minimum height to the position which corresponds to the static equilibrium, when the vertical velocity of the gravity centre assumes a relative maximum value. In this interval the resultant of the aerodynamic forces, which is still directed upward, acts in the same direction as that of the upward translational motion of the deck and then produces an effect of amplification of the same motion.
- In the time interval between instants C and D the gravity centre of the deck still moves upward until it reaches the position of maximum height (within the considered oscillation cycle), when the vertical velocity of the gravity centre vanishes again. In this interval the magnitude of the resultant of the aerodynamic forces switches from positive values to negative values (close to zero). For most of this interval the above resultant acts in the same direction as that of the upward translational motion of the deck and then still amplifies the translational motion of the deck.
- In the time interval between the instants D and E the gravity centre of the structure inverts the direction of the translational motion and passes from the position of maximum height to the position which corresponds to the static equilibrium, when the vertical velocity of the gravity centre assumes a relative minimum value. In this last portion of the oscillation cycle the resultant of the aerodynamic forces starts to grow one more from negative values (close

to zero). In this interval the above resultant acts in opposition to the downward translational motion of the deck and then provides a damping effect of the same translational motion.

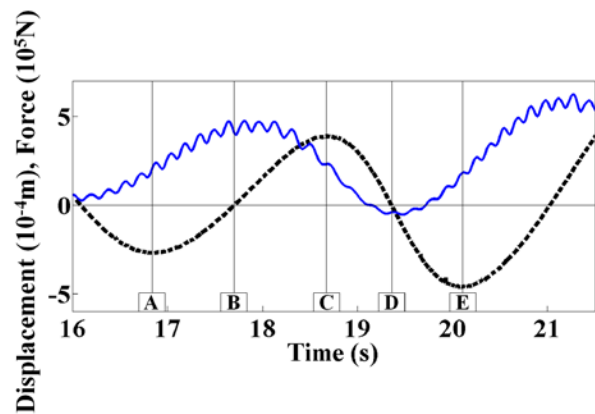


Fig. 8: Time histories of the resultant of the unit-area forces exerted by the fluid on the deck surface (blue) and of the infinitesimal vertical displacement of the centre of gravity of the deck (black, dashed)

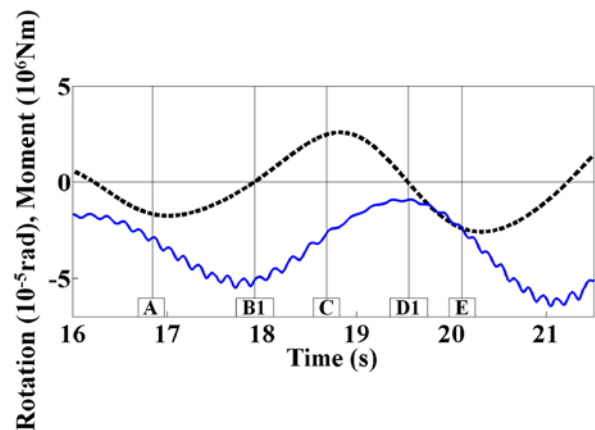


Fig. 9: Time histories of the aerodynamic twisting moment (blue) and of the infinitesimal deck rotation (black, dashed)

By observing Fig. 8 it can be deduced that, in the time intervals A-B and D-E of the considered cycle, the force resultant acts against the vertical motion of the centre of gravity whereas, during the time interval B-D, the same resultant acts in favour of the translational motion. The integral of the work performed by the force resultant over the infinitesimal displacement of the centre of gravity during the time interval B-D is around equal to 260 kJ. This value is found to be considerably higher, in modulus, than the value obtained by adding the integral of the work performed during the time interval A-B (around -100 kJ) and the integral of the work performed during the time interval D-E (around -60 kJ). It follows that the net input of energy (roughly 100 kJ) of the aerodynamic resultant force to the translational motion is to

destabilise the motion itself.

Similar considerations apply to the effect of the twisting moment produced by the above resultant force to the rotational motion. Fig. 9 shows that, in the time intervals A-B1 and D1-E, the above moment acts in favour of the rotational motion of the deck, thus providing an amplification effect of the motion itself. By contrast, during the time interval B1-D1, the twisting moment acts against the rotational motion and, consequently, produces a damping effect of the motion itself. The integral of the work performed by the twisting moment over the infinitesimal deck rotation during the entire cycle A-E is around equal to 25 kJ. It can be deduced that the net input of energy of the aerodynamic twisting moment to the rotational motion is to destabilise the motion itself.

On the basis of the above consideration, it is possible to conclude that the reason for the onset of the instability resides in the fact that there are some temporal fractions, within each of the first oscillation cycles, in which the aerodynamic field provides both the translational and the rotational motion with a higher supply of energy than that subtracted from the deck motion in the rest of the cycle.

After the instability of the roto-translational motion has been triggered, the maximum amplitude of the rotation angle progressively increases. As shown in the following subsection, once the above angle exceeds a threshold value the leading edge recirculation bubble, which pulsates in the onset phase just described, starts to drift along the deck surface. From this point on, the modalities by which the oscillations amplify are different to those described before in the present subsection.

E. Post-Critical Flutter Mechanism

Below the amplification mechanism of coupled flutter is shown. For this purpose, the evolution of the aerodynamic fields and the structural motion developed for a wind speed $U = 87.4$ m/s ($U_\theta = 7.0$) is investigated during a cycle of structural oscillations in which the deck exhibits large amplitudes of vibration. Figs. 10-13 show the fluid velocity field which form around the deck in four time instants T1-T4 included in $\frac{1}{2}$ of the above cycle. It is intended by $\frac{1}{2}$ cycle the time interval delimited by the instant when the gravity centre of the downward moving structure corresponds to the static equilibrium position of the structure's centre of gravity and the instant when the gravity centre of the upward moving structure corresponds to the static equilibrium position of the structure's centre of gravity. Figs. 14-17 show the distribution of the surface normal unit-area forces exerted by the fluid on the deck (aerodynamic forces) in the same time instants.

- In the first of the four considered instants a downward translation and a clockwise rotation of the deck is ongoing. The angle of attack is sufficiently high to cause the flow detachment near the leading edge. In Fig. 10 the vortex formed immediately downline this detachment zone is shown. In Fig. 14 the distribution of the aerodynamic forces can be seen. The resultant of these forces is an upward force directed normally to the upper surface of the deck. In this instant, this resultant acts in opposition to the downward

velocity of the gravity centre and, therefore, provides a damping effect on the translational vertical motion of the deck. The point of application of the resultant is placed near the centre of the vortex, in an extremely far position from the mid-chord point of the deck cross-section. This resultant gives rise to a clockwise twisting moment which prevails against the elastic and the damping moment acting in the same instant and, together with the inertial torque, leads to an amplification of the clockwise rotation of the deck.

- In Fig. 11 it can be seen that, compared to the previous instant, the vortex has drifted along the upper surface toward the trailing edge. This change of position is accompanied with a growth in the dimensions of the vortical formation. By observing Fig. 15 it can be seen that an overall increase of the aerodynamic forces is associated to the growth of the vortex. The point of application of the resultant, placed near the centre of the vortex, has got close to the mid-chord point of the deck cross-section. The effect produced by the increase of the intensity of the resultant prevails against the effect produced by the change of its point of application, causing an increase of the intensity of the clockwise twisting moment due to this resultant. Consequently this twisting moment acts in opposition to the elastic and the damping moment and, together with the inertial torque, produces a further amplification of the clockwise rotation of the deck. As well as in the previous instant, the resultant of the aerodynamic forces acts in opposition to the downward translational motion of the gravity centre and, therefore, still provides a damping effect on the motion itself.
- By examining Fig. 12 it can be seen that, compared to the previous instant, the vortex has further drifted along the upper surface, getting close to the trailing edge. In Fig. 16 it is seen that an overall increase of the aerodynamic forces corresponds to the growth of the vortex. At the same time it can be seen that the point of application of the resultant has got closer to the mid-chord point of the deck cross-section. The effect produced by the change of position of the resultant's point of application prevails against the effect produced by the increase of its intensity, causing a decrease of the intensity of the clockwise twisting moment due to this resultant. The aerodynamics twisting moment continues to act in opposition to the elastic and the damping moment, but its intensity has reduced compared to the previous instant.
- In the latest of the four considered instants the inversion of the translational and rotational motion of the deck has taken place. In Fig. 13 it is shown that the vortex still drifts along the upper surface till reaching the trailing edge. Fig. 17 shows the distribution of the aerodynamic forces. The resultant of the these forces slightly decreases compared to the previous instant. The point of application of the resultant, previously placed between the leading edge and the mid-chord point, is now placed between the mid-chord point and the trailing edge. Consequently the moment due to the resultant changes sign and, as a result of the

simultaneous change in the rotation direction of the deck, acts in the same direction as that of the angular velocity. The resultant of the aerodynamic forces acts in the same direction as the upward velocity of the gravity centre, so that it provides a contribution in the amplification of the upward translational motion of the deck.

By examining Figs. 10-13 and Figs. 14-17 it can be deduced that the instability amplification is due to the formation and drift of large-scale vortices on the surface of the deck. From the simulation it is possible to deduce that the resultant of the surface normal unit-area forces exerted by the fluid on the deck surface moves with the vortical formation generated at the leading edge. The point of application of this resultant is placed at the vortical formation. Therefore, the movement of this resultant with respect to the shear centre gives rise to a twisting moment which varies in intensity and direction during the deck oscillation. In particular, the sign of this twisting moment is found to be always coherent with the sign of the instantaneous angular velocity. Consequently, there is a continuous supply of energy from the fluid dynamic field to the structure, that constitutes the reason for the amplification of the instability of the torsional motion. The integral of the work performed by the resultant of the aerodynamic forces

over the infinitesimal displacement of the centre of gravity during the entire cycle is positive. As a consequence, the net effect of the resultant on the translational motion of the deck is to amplify the above-mentioned motion and provide a destabilising contribution.

F. Aeroelastic Optimization of the Deck

The proposed simulation model is used in order to evaluate the aero-elastic stability of the Forth Road Bridge deck in a configuration modified by the introduction of a couple of sloping barriers at the windward and leeward bridge deck edges. In Fig. 18 the geometric characteristics of the Forth Road Bridge deck in the modified configuration are shown. The wind barriers are 2.0 m high and inclined by 45 degrees with respect to the vertical direction. The fluid-structure interaction for the modified configuration is simulated by means of a block-structured grid made up of 276520 cells.

In order to compare the static behaviour of the two different configurations of the Forth Road Bridge deck (current and modified configuration), the static aerodynamic coefficients are computed for various Reynolds number ($1.39 \times 10^7 < Re < 1.95 \times 10^8$).

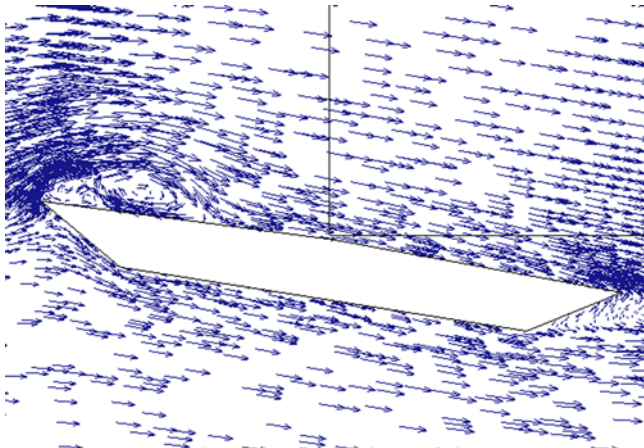


Fig. 10: Fluid velocity field around the deck at T1

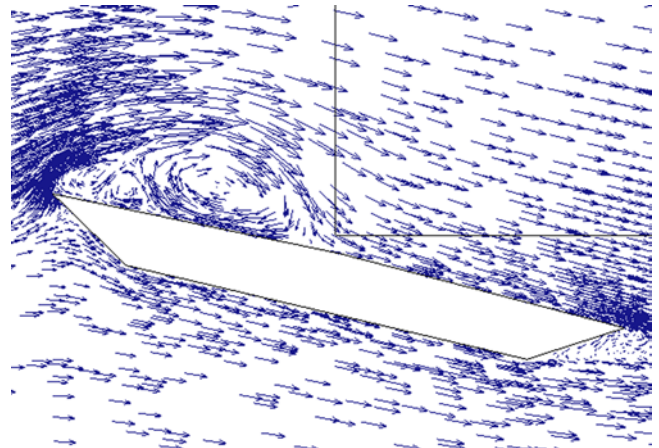


Fig. 11: Fluid velocity field around the deck at T2

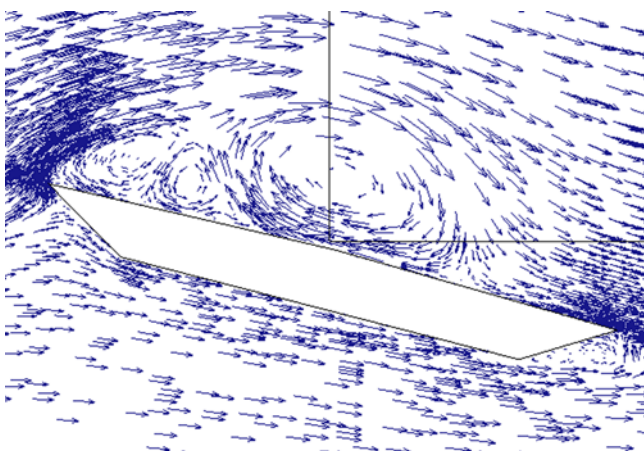


Fig. 12: Fluid velocity field around the deck at T3

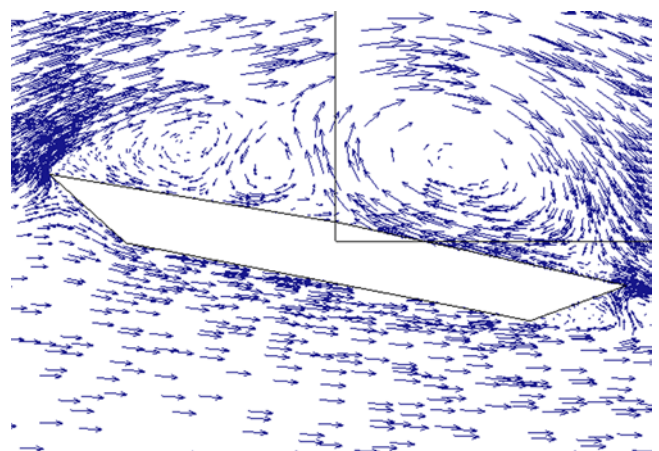


Fig. 13: Fluid velocity field around the deck at T4

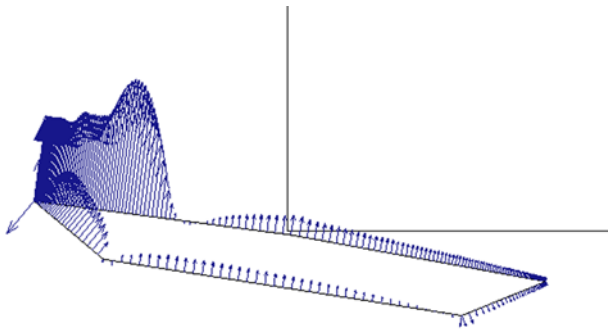


Fig. 14: Distribution of the unit-area fluid forces at T1

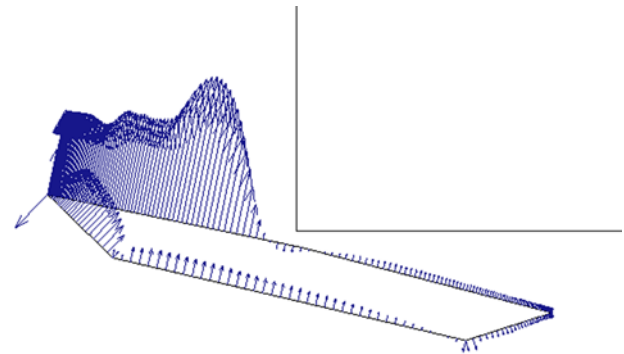


Fig. 15: Distribution of the unit-area fluid forces at T2

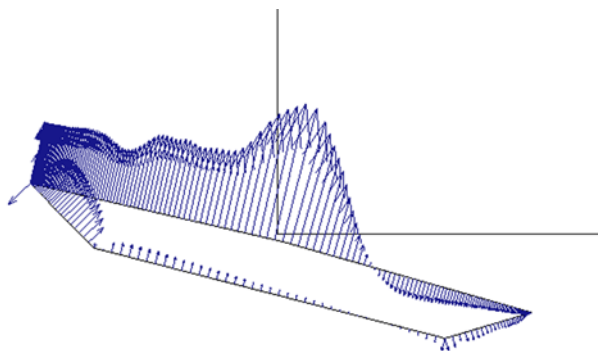


Fig. 16: Distribution of the unit-area fluid forces at T3

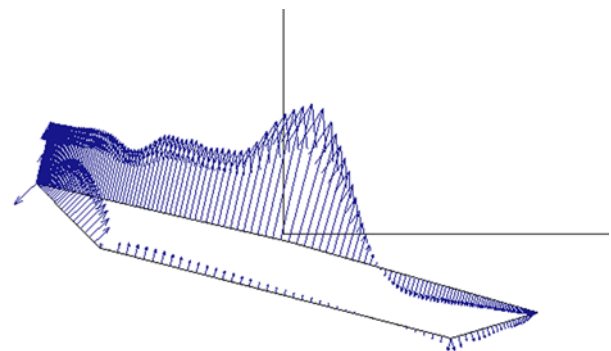


Fig. 17: Distribution of the unit-area fluid forces at T4

The obtained time-averaged drag coefficient $C_D = F_D / (0.5 \rho U^2 D)$ (in which F_D is the drag force exerted by the fluid on the structure, U the undisturbed wind velocity, D the depth of the deck cross-section and ρ the fluid density), the time-averaged lift coefficient $C_L = F_L / (0.5 \rho U^2 B)$ (in which F_L is the lift force exerted by the fluid on the structure and B the width of the deck cross-section) and the time-averaged moment coefficient $C_M = M / (0.5 \rho U^2 B^2)$ (in which M is the aerodynamic moment exerted by the fluid on the structure) for the two different configurations of the Forth Road Bridge deck are given in Table 2. For each of the examined quantities, the first number reported in this table refers to the simulation performed for $Re = 1.39 \times 10^7$, whilst the second number refers to the simulation performed for $Re = 1.95 \times 10^8$. From this table it can be deduced that, compared to its current configuration, the introduction of the sloping barriers causes a slight decrease in the drag coefficient, a slight increase in the lift coefficient and a considerable decrease in the moment coefficient.

Table2: Time averaged drag, lift and moment coefficients and Strouhal number of the Forth Road Bridge deck in the current and the modified configuration

	Current	Modified
Drag coefficient (C_D)	0.578 ÷ 0.644	0.379 ÷ 0.441
Lift coefficient (C_M)	-0.584 ÷ -0.685	-1.951 ÷ -2.444
Moment coefficient (C_M)	-0.391 ÷ -0.445	-0.018 ÷ -0.043
Strouhal number (St)	0.23 ÷ 0.25	0.24 ÷ 0.27

In addition to the time-averaged static coefficients, Table 2 lists also the Strouhal number values computed for the Forth Road bridge deck in both current and modified configurations. For the deck in its current configuration, the numerical simulations provide slightly variable values for the Strouhal number which are between 0.23 and 0.25; for the deck in the modified configuration, the numerical simulations provide slightly higher values for the Strouhal number which are between 0.24 and 0.27. From the values of the Strouhal number, the critical flutter wind velocity for which the Vortex Induced Vibration (VIV) instability occurs are calculated by means of the expression $U_{VIV} = (\Omega_y D) / St$, where Ω_y is the

natural heaving frequency of the deck. It follows that the critical VIV wind velocity for the deck in the modified configuration is slightly lower (2.2 m/s) than the critical VIV wind velocity for the deck in its current configuration (2.3 m/s). From this comparison it results that the modification of the cross-section of the Forth Road Bridge deck through the introduction of the sloping barriers causes only a slight deterioration in the VIV instability.

With the purpose of characterising the flutter type of the modified configuration, the angle Ψ defined as the phase-lag of the heaving response to the torsional response of the structure is used. In the case under examination, this angle is $\Psi = -29^\circ$. It is thus concluded that, in this case, the Forth Road Bridge deck is prone to a TB coupled flutter in which the torsional fundamental mode still dominates but to which the heaving fundamental mode contributes to a greater extent than

in the case related to the bridge deck in the current configuration.

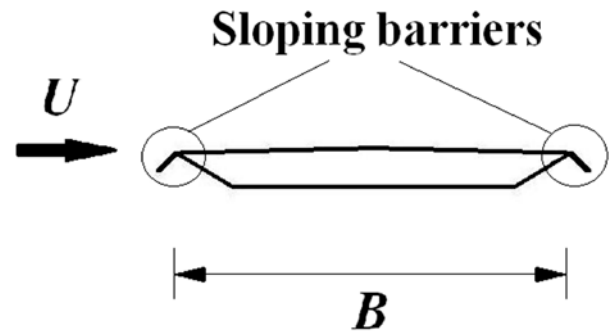


Fig. 18: Geometry of the Forth Road Bridge deck cross-section in the modified configuration

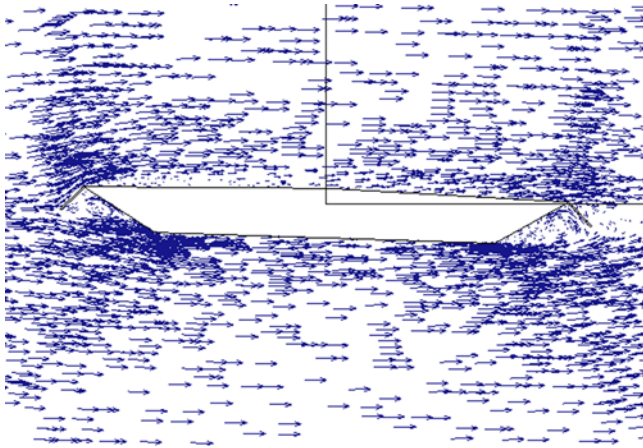


Fig. 19: Fluid velocity field around the deck at T1 (configuration modified through sloping barriers)

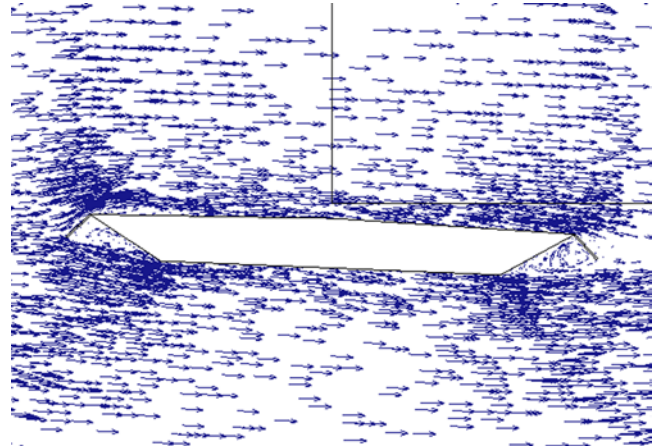


Fig. 20: Fluid velocity field around the deck at T2 (configuration modified through sloping barriers)

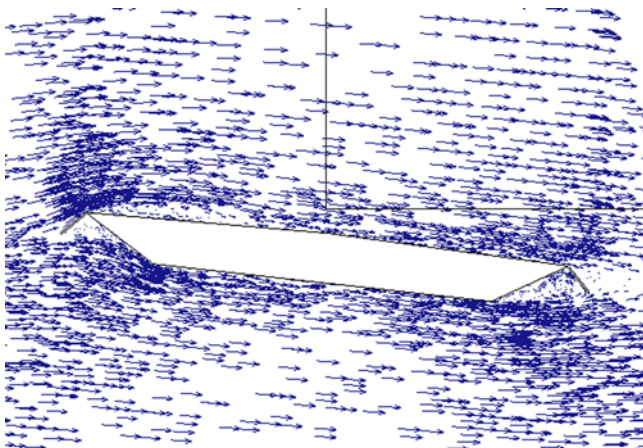


Fig. 21: Fluid velocity field around the deck at T3 (configuration modified through sloping barriers)

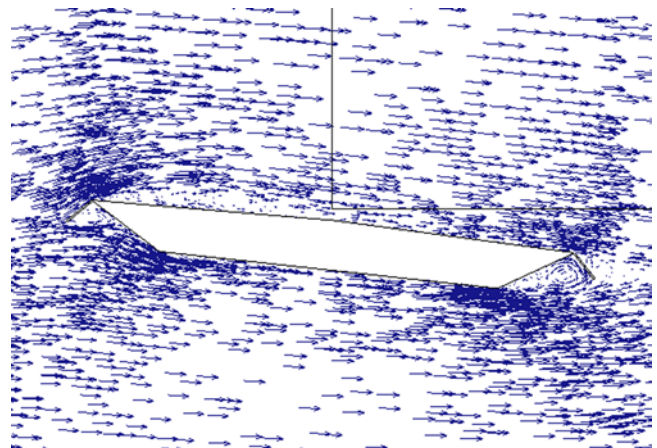


Fig. 22: Fluid velocity field around the deck at T4 (configuration modified through sloping barriers)

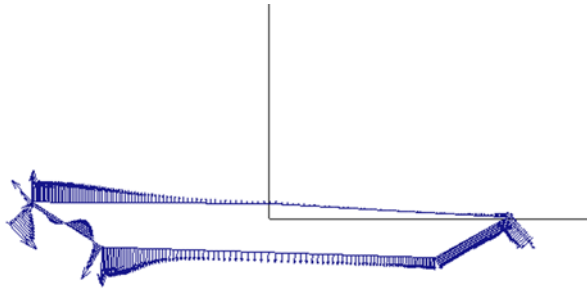


Fig. 23: Distribution of the unit-area fluid forces at T1 (configuration modified through sloping barriers)

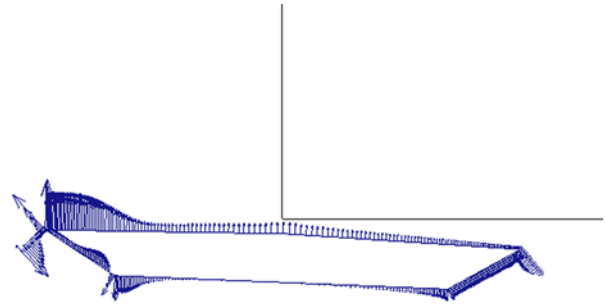


Fig. 24: Distribution of the unit-area fluid forces at T2 (configuration modified through sloping barriers)

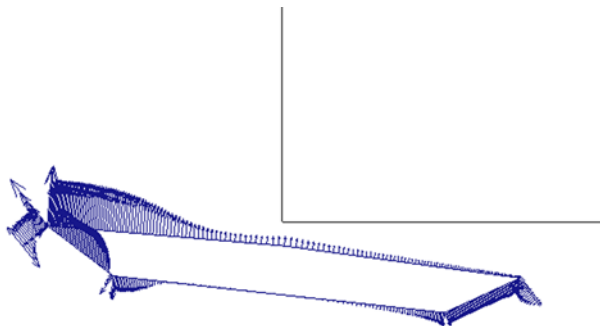


Fig. 25: Distribution of the unit-area fluid forces at T3 (configuration modified through sloping barriers)

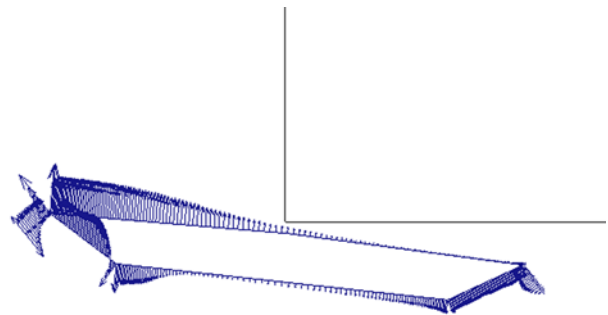


Fig. 26: Distribution of the unit-area fluid forces at T4 (configuration modified through sloping barriers)

The critical flutter wind velocity value is $U^* = 82.6$ m/s ($U_{\theta}^* = 6.62$), which is slightly higher than the one identified for the deck in its current configuration. Therefore this modification is to be considered effective in the improvement of the aero-elastic stability of the deck. Moreover, as observed with regard to the current configuration it is found that, for wind velocity values equal or greater than the critical flutter wind velocity value, the frequencies of the rotational and vertical wind-induced motion synchronise on a common frequency.

Figs. 19-22 show the fluid velocity field which form around the deck in four time instants T1-T4 included in $\frac{1}{2}$ of an oscillation cycle when flutter oscillations have been already developed. Figs. 23-26 show the distribution of the surface normal unit-area forces exerted by the fluid on the deck (aerodynamic forces) in the same time instants. As a result of the introduction of the sloping barriers, a remarkable decrease in the amplitudes of the oscillations which develop during the evolution of the phenomenon is observed. This decrease in the amplitudes of the vibrations is due to the fact that, as a result

of the introduction of the sloping barriers, the flow detachment near the leading edge is limited compared to the early case (current configuration) and, consequently, there is a considerable delay in the formation and drifting of large vortical formations along the surface of the deck. It is thus concluded that the aerodynamic modification can be considered effective in the mitigation of the amplitudes of the vibration which develop during the evolution of the flutter instability.

IV. CONCLUSION

In this work the aeroelastic stability of long-span bridge decks has been numerically investigated. A simulation model has been presented by which the aerodynamic fields and the structural motion are simultaneously and jointly simulated. The validation of the numerical model has been performed by comparing the numerical results with those of an experimental campaign, in terms of critical flutter wind velocity and root-mean-square of the deck rotational displacements, and has been used to investigate the aeroelastic stability of the Forth

Road Bridge deck.

A profound insight into the onset and the amplification mechanisms of coupled flutter for long-span bridge decks is proposed. It has been demonstrated that the reason for the onset of the instability resides in the fact that there are some temporal fractions, within each of the first oscillation cycles, in which the aerodynamic field provides both the translational and the rotational motion of the deck with a higher supply of energy than that subtracted from the motion itself in the rest of the cycle. Once the instability has been triggered, the amplitudes of vibrations increase at each cycle until the leading edge recirculation bubble, which pulsates for small oscillation amplitudes, bursts producing large vortical formations which drift along the upper side of the bridge deck. The drifting of this vortical formations has been found to be the reason for the amplification of the instability. It has been shown that the sign of the twisting moment produced by the aerodynamic field on the structure is always coherent with that of the rotation. Consequently, there is a continuous supply of energy from the fluid dynamic field to the structure, that constitutes the key to the amplification of the instability of the torsional motion.

The numerical model has been used to test the effectiveness of a small aerodynamic modification of the deck cross-section on the aeroelastic stability of the deck. It has been shown that the introduction of a couple of sloping barriers at the windward and leeward bridge deck edges causes an increase in the critical flutter wind velocity and a reduction in the amplitudes of vibrations which develop during the evolution of the phenomenon. This decrease in the amplitudes of the vibrations is due to the fact that, as a result of the above modification, there is a delay in the formation and drifting of large vortical formations along the surface of the deck.

REFERENCES

- [1] E. Dowell, *A Modern Course in Aeroelasticity: Fifth Revised and Enlarged Edition*. Springer, 2014, pp. 285-347.
- [2] A. Larsen, "Aerodynamics of the Tacoma Narrows Bridge - 60 Years Later", *Structural Engineering International*, vol. 10, no. 4, pp. 243-248, Nov. 2000.
- [3] F. L. Haan, "The effects of turbulence on the aerodynamics of long-span bridges", PhD dissertation, Dept. Aeros. and Mech. Eng., Univ. of Notre Dame, Indiana, 2000.
- [4] J. B. Frandsen, "Numerical bridge deck studies using finite elements. Part I: flutter", *J. Fluid Struct.*, vol. 19, no. 2, pp. 171-191, Feb. 2004.
- [5] M. Matsumoto, H. Matsumiya, S. Fujiwara, and Y. Ito, "New consideration on flutter properties based on step-by-step analysis", *J. Wind Eng. Ind. Aerod.*, vol. 98, no. 12, pp. 429-437, Aug.-Sep. 2010.
- [6] R. H. Scanlan and J. J. Tomko, "Airfoil and bridge deck flutter derivatives", *J. Eng. Mech. Div.-ASCE*, vol. 97, pp. 1717-1737, Dec. 1971.
- [7] M. A. Astiz, "Flutter stability of Very Long Suspension Bridges", *J. Bridge Eng.*, vol. 3, no. 3, pp. 132-139, Aug. 1998.
- [8] R. P. Selvam, S. Govindaswamy, and H. Bosch, "Aeroelastic analysis of bridges using FEM and moving grids", *Wind Struct.*, vol. 5, no. 2_3_4, pp. 257-266, 2002.
- [9] I. Robertson, S. J. Sherwin, and P. W. Bearman, "Flutter instability prediction techniques for bridge deck sections", *Int. J. Numer. Meth. Fl.*, vol. 43, no. 10-11, pp. 1239-1256, Dec. 2003.
- [10] A. L. Braun and A. M. Awruch, "Finite element simulation of the wind action over bridge sectional models: Application to the Guamà River Bridge (Parà State, Brazil)", *Finite Elem. Anal. Des.*, vol. 44, no. 3, pp. 105-122, Jan. 2008.
- [11] S. Oka and T. Ishihara, "Numerical study of aerodynamic characteristics of a square prism in a uniform flow", *J. Wind Eng. Ind. Aerod.*, vol. 97, no. 11-12, pp. 548-559, Dec. 2009.
- [12] L. Brun and S. Khris, "The validity of 2D numerical simulations of vortical structures around a bridge deck", *Math. Comput. Model.*, vol. 37, no. 7-8, pp. 795-828, Apr. 2003.
- [13] F. Cioffi and F. Gallerano, "From rooted to floating vegetal species in lagoons as a consequence of the increases of external nutrient load: An analysis by model of the species selection mechanism", *Appl. Math. Model.*, vol. 30, no. 1, pp. 10-37, Jan. 2006.
- [14] Y. Cheng, F. S. Lien, E. Yee, and R. Sinclair, "A comparison of Large Eddy Simulations with a standard $k-\epsilon$ Reynolds-averaged Navier-Stokes model for the prediction of a fully developed turbulent flow over a matrix of cubes", *J. Wind Eng. Ind. Aerod.*, vol. 91, no. 11, pp. 1301-1328, Nov. 2003.
- [15] G. Cannata, F. Lasaponara, and F. Gallerano, "Non-Linear Shallow Water Equations numerical integration on curvilinear boundary-conforming grids", *WSEAS Transactions on Fluid Mechanics*, vol. 10, pp. 13-25, 2015.
- [16] Md. N. Haque, H. Katsuchi, H. Yamada, and M. Nishio, "Flow field analysis of a pentagonal-shaped bridge deck by unsteady RANS", *Eng. Appl. Comp. Fluid*, vol. 10, no. 1, pp. 1-16, 2016.
- [17] F. Gallerano, G. Cannata, and F. Lasaponara, "A new numerical model for simulations of wave transformation, breaking and long-shore currents in complex coastal regions", *Int. J. Numer. Meth. Fl.*, vol. 80, no. 10, pp. 571-613, Apr. 2016.
- [18] F. Gallerano, G. Cannata, and F. Lasaponara, "Numerical simulation of wave transformation, breaking and runup by a contravariant fully non-linear Boussinesq equations model", *J. Hydrodynam. B*, vol. 28, no. 3, pp. 379-388, Jun. 2016.
- [19] Z. Zhu, M. Gu, and Z. Chen, "Wind tunnel and CFD study on identification of flutter derivatives of a long-span self-anchored suspension bridge", *Comput. Aided Civil Infrastruct. Eng.*, vol. 22, no. 8, pp. 514-554, Nov. 2007.
- [20] S. De Miranda, L. Patrino, F. Ubertini, and G. Vairo, "On the identification of flutter derivatives of bridge decks via RANS turbulence models: Benchmarking on rectangular prisms", *Eng. Struct.*, vol. 76, pp. 359-370, Oct. 2014.
- [21] F. Nieto, D. M. Hargreaves, J. S. Owen, and S. Hernandez, "On the applicability of 2D URANS and SST $k-\omega$ turbulence model to the fluid-structure interaction of rectangular cylinders", *Eng. Appl. Comp. Fluid*, vol. 9, no. 1, pp. 157-173, 2015.
- [22] M.W. Sarwar and T. Ishihara, "Numerical study on suppression of vortex-induced vibrations of box girder bridge section by aerodynamic countermeasures", *J. Wind Eng. Ind. Aerod.*, vol. 98, no. 12, pp. 701-711, Dec. 2010.
- [23] C. Mannini, A. M. Marra, and G. Bartoli, "VIV-galloping instability of rectangular cylinders: review and new experiments", *J. Wind Eng. Ind. Aerod.*, vol. 132, pp. 109-124, Sep. 2014.
- [24] C. Mannini, A. Soda, and G. Schewe, "Unsteady RANS modelling of flow past a rectangular cylinder: Investigation of Reynolds number effects", *Comput. Fluids*, vol. 39, no. 9, pp. 1609-1624, Oct. 2010.
- [25] K. Shimada and T. Ishihara, "Predictability of unsteady two-dimensional $k-\epsilon$ model on the aerodynamic instabilities of some rectangular prisms", *J. Fluid Struct.*, vol. 28, pp. 20-39, Jan. 2012.
- [26] C. Hertel, M. Schumichen, S. Lobig, J. Frohlich, and J. Lang, "Adaptive large eddy simulation with moving grids", *Theor. Comp. Fluid Dyn.*, vol. 27, no. 6, pp. 817-841, Nov. 2013.
- [27] F. R. Menter, "Review of the shear-stress transport turbulence model experience from an industrial perspective", *Int. J. Comput. Fluid D.*, vol. 23, no.4, pp. 305-316, Apr. 2009.
- [28] L. Li, S. J. Sherwin, and P. W. Bearman, "A moving frame of reference algorithm for fluid/structure interaction of rotating and translating bodies", *Int. J. Numer. Meth. Fl.*, vol. 38, no. 2, pp. 187-206, Jan. 2002.
- [29] R. J. Spiteri and S. J. Ruuth, "A new class of optimal high-order strong-stability preserving time discretization methods", *SIAM J. Numer. Anal.*, vol. 40, no. 2, pp. 469-91, 2002.
- [30] F. Gallerano and G. Cannata, "Central WENO scheme for the integral form of contravariant shallow-water equations", *Int. J. Numer. Meth. Fl.*, vol. 67, no. 8, pp. 939-959, Nov. 2011.

- [31] F. Gallerano, G. Cannata, and M. Tamburrino, "Upwind WENO scheme for Shallow Water Equations in contravariant formulation", *Comput. Fluids*, vol. 62, pp. 1-12, Jun. 2012.
- [32] F. Gallerano, G. Cannata, and M. Villani, "An integral contravariant formulation of the fully non-linear Boussinesq equations", *Coast. Eng.*, vol. 83, pp. 119-136, Jan. 2014.
- [33] L. Uyttersprot, "Inverse Distance Weighting Mesh Deformation", M.S. thesis, Delft Univ. of Tech., Dept. Aerod., Delft, Netherlands, 2014.
- [34] F. Menter, J. Carregal Ferreira, T. Esch, and B. Konno, "The SST Turbulence Model with Improved Wall Treatment for Heat Transfer Predictions in Gas turbines", in *Proc. of the Int. Gas Turbine Cong.*, Tokyo, 2003, pp. 1-7.